International Journal of
Network Dynamics and Intelligence (IJNDI)

Scilight

Article

Check for updates

Denoising of Microseismic Data Using U-Net Network with Residual Hybrid Dilated Convolutional Space Attention Mechanism

Huashuai Cui [1,2,3,4], Fei Han [1,2,3,4,*], Yuhang Sun [1,2,3,4], and Huanjun Chen [1,2,3,4]

[1] National Key Laboratory of Continental Shale Oil, Northeast Petroleum University, Daqing 163318, China
[2] Artificial Intelligence Energy Research Institute, Northeast Petroleum University, Daqing 163318, China
[3] Heilongjiang Provincial Key Laboratory of Networking and Intelligent Control, Northeast Petroleum University, Daqing 163318, China
[4] Research Center for Mathematics and Interdisciplinary Sciences, Northeast Petroleum University, Daqing 163318, China
* Correspondence: tomcumt@126.com
Received: 14 January 2026; Revised: 2 March 2026; Accepted: 5 May 2026; Published: 22 June 2026

Abstract: Noise reduction plays a pivotal role in enhancing the signal-to-noise ratio (SNR) of microseismic data during the preprocessing stage. However, due to the heterogeneous nature and high complexity of noise sources, conventional model-driven denoising methods frequently exhibit suboptimal performance, thereby compromising the fidelity and reliability of downstream microseismic processing tasks. Moreover, while deep learning-based approaches have shown promise for microseismic noise suppression, the resulting models often exhibit limited generalization capability and insufficient preservation of physically meaningful signal features. To address these challenges, this study introduces RD-SAUNet—a novel U-Net–based architecture incorporating hybrid dilation convolutions and a residual spatial attention mechanism. Built upon the foundational U-type convolutional neural network (U-Net) framework, RD-SAUNet integrates three key innovations: (i) residual connections to facilitate gradient flow and accelerate training convergence; (ii) a spatial attention mechanism (SAM) that adaptively emphasizes discriminative signal features while suppressing spurious noise; and (iii) hybrid dilation convolutions that expand the receptive field to capture broader contextual information without significantly increasing computational overhead. Collectively, these design choices enhance both model generalizability and signal fidelity. The proposed method is rigorously evaluated on both synthetic and field-collected microseismic datasets and benchmarked against state-of-the-art denoising techniques. Experimental results confirm that RD-SAUNet achieves robust suppression of random noise, yields substantial SNR improvement, and faithfully preserves the intrinsic temporal-spectral characteristics essential for accurate microseismic event detection and characterization.

Keywords: micro-seismic; noise suppression; spatial attention mechanism; residual network; dilated convolution; signal-to-noise ratio

1. Introduction

In microseismic monitoring, due to environmental noise interference, the measured microseismic data is frequently polluted by the noise. Noise reduction of microseismic data is an important step in microseismic data preprocessing, which is the premise and foundation of subsequent event identification, initial pick-up, source location and source mechanism inversion [1–3]. Until now, researchers have proposed numerous noise reduction algorithms, which can be roughly divided into two types: model-driven noise reduction methods [4–7] and data-driven noise reduction methods [8]. The former is realized by optimization algorithms using signal processing theory or statistical characteristics of interference noise in microseismic data. The latter relies on automatically learning noise reduction strategy from extensive training data without relying on the specific physical modeling of the noise and signal.

Traditional model-driven methods of microseismic noise suppression include continuous wavelet transform (CWT) [9], Shearlet transform [10], wavelet packet transform (WPT), empirical mode decomposition (EMD) [3,11], and variational mode decomposition (VMD) [12]. For example, ref. [13] has applied adaptive filtering to microseismic data based on the synchronous compressed CWT. This approach provides higher resolution than the traditional wavelet transform, avoids certain artifacts, and effectively removes most of the noise from small-amplitude signals. An improved adaptive F-K filtering method has been proposed in [14], which addresses the issue of false in-phase axis and effectively removes both coherent and random noise. Similarly, a denoising filter has been designed based on the Shearlet transform domain in [15], where an automatic phase selector p, based on high-order statistical criteria, is adopted to process and analyze continuously recorded single channel microseismic data. More recently, an adaptive microseismic signal denoising method based on VMD and energy entropy has

been proposed in [12]. However, the data priors assumed by these methods are only approximations of the actual microseismic data. Furthermore, they rely on many manually set parameters, which increases manual effort and introduces uncertainty into the denoising process.

In recent years, deep learning-based noise suppression has been widely adopted due to its powerful nonlinear composite mapping capability. It effectively addresses the modeling inaccuracies and parameter uncertainties inherent in traditional denoising methods [16, 17], which often stem from insufficient prior knowledge. By leveraging multi-layer convolutional networks, the approach extracts salient features from microseismic data and constructs an adaptive denoising model [18,19]. The most widely used denoising method for microseismic data is filtering based on convolutional neural network (CNN) [20]. For example, an event detection method based on CNN has been developed in [21] to automatically classify microseismic events. CNNs have been used to jointly perform interpolation of two-dimensional coherent seismic datasets and random noise attenuation in [22]. In addition, both CNN and U-Net are commonly used for image denoising and image segmentation tasks. CNNs have been applied in [23] to remove random noise from seismic data, achieving better performance than traditional methods. The original CNN model has been extended in [24], where a CNN for random noise attenuation in seismic data is constructed, and the activation function is replaced with exponential linear units to enhance the robustness. An end-to-end noise residual learning network via denoising convolutional neural network (DnCNN) has been constructed to denoise microseismic data more efficiently in [25]. A method has been proposed in [26] based on data augmentation and U-Net to suppress random noise in seismic data, which provides a solution to the data labeling in deep learning. To addrss the generalization problem, a residual block has been added to U-Net in [27], which achieves a denoising effect while preserving the effective signal. A multilayer U-Net has been used in [28] to learn the sparse characteristics in both time and frequency domain for microseismic data denoising. Finally, a full-CNN noise reduction method has been proposed in [18] to learn different types of noise via the residual learning strategy, and experiments show that this method can effectively suppress mixed noises.

The denoising efficiency of CNNs is considerably constrained by their limited feature extraction capacity and the significant discrepancies between synthesized training data and real-world microseismic signals. Integrating attention mechanisms with CNN architectures effectively mitigates the loss of fine-grained input features, thereby enhancing noise suppression performance[29,30]. Building on this concept, AD-Net [31] successfully extracts noise components from complex backgrounds and achieves notable denoising performance. Furthermore, a deep CNN incorporating global context awareness and an attention mechanism has been introduced for seismic data denoising in [32], which effectively suppresses noise while preserving critical local structural details. However, the feedforward direct-connection architecture of CNNs lacks a dedicated pathway for transmitting spatial details from deeper layers back to shallower layers. As a result, attention modules can only recalibrate feature maps within the current layer, without the ability to leverage high-level semantic information from the decoder to guide the selection of shallow spatial features. This inherent limitation results in denoising models that adapt poorly to microseismic signals, which are often characterized by variable waveforms and indistinct boundaries.

Owing to its unique skip connection architecture, U-Net has been widely adopted in image processing, as well as in the processing and analysis of seismic and microseismic signals [33], demonstrating outstanding effectiveness [34–36]. However, the conventional U-Net model still has problems such as limited generalization ability and insufficient retention of effective signal components. The primary challenge in attenuating random noise in microseismic data lies in the inherently low signal-to-noise ratio (SNR), which makes it difficult to distinguish effective signals from noise. This challenge not only complicates the denoising process but also increases the risk of losing essential signal components during noise suppression. Therefore, there is a pressing need to develop an effective and accurate method for random noise attenuation in microseismic data. Motivated by these considerations, this paper proposes an improved U-Net architecture by integrating a fusion attention mechanism, which addresses the issue of inadequate feature extraction in microseismic data analysis. The contributions of this article are summarized as follows.

1. A Residual-Spatial Attention Mechanism (RSAM) is proposed for microseismic random noise attenuation. The spatial attention mechanism focuses on the key spatial regions in the signal by dynamically allocating weights. Skip connections are used to enhance the multi-level feature fusion ability of the module, thereby avoiding the loss of key details. By embedding RSAM into the U-Net architecture, the feature maps of the current layer can be spatially recalibrated, while the high-level semantic information from the decoder is leveraged to guide the selection of shallow features in a top-down manner. This significantly enhances the model's ability to recover effective wave groups in microseismic signals, which are often characterized by variable waveforms and indistinct boundaries. Moreover, the symmetric skip-connection structure of U-Net provides the precise interaction pathway that RSAM requires, effectively upgrading the attention mechanism

from local feature enhancement to global–local collaborative noise suppression, thereby overcoming the inherent limitation of unidirectional information flow in standard CNNs.

2. Hybrid dilated convolution is employed to increase the receptive field for extracting global context information. U-Net's skip connections primarily ensure spatial localization accuracy, while hybrid dilated convolution is designed to expand the semantic receptive field. Together, they enable the encoder to capture global contextual information without resolution loss and allow the decoder to recover fine details via skip connections. This forms a collaborative mechanism of "global understanding and local refinement," which fundamentally overcomes the local receptive field limitation inherent in traditional CNNs.

The remainder of this article is organized as follows. In Section II, the RD-SAUNet is proposed. The effectiveness of this proposed method is then validated using synthetic and field samples in Section III and IV, where a series of carefully designed comparisons are used to verify the superiority of RD-SAUNet. Finally, the conclusions are presented in Section V.

2. Method Principle

2.1. Denoising Principle

Microseismic data denoising is the process of recovering clean microseismic signals from their noisy counterparts. The microseismic signals captured by geophones contain both meaningful information and a significant amount of random noise. The microseismic signal can be regarded as the sum of the effective signal and noise interference, which can be represented by the following simple formula:

$$y = x + n \tag{1}$$

where y is training samples of micro-seismic data containing noise; x is training samples of clean microseismic data; and n is random Gaussian noise.

In this paper, the noise estimation $\hat{n}$ is derived using a residual learning strategy during training. The denoised microseismic data $\hat{x}$ is then obtained by subtracting the noise estimation $\hat{n}$ from the microseismic data y, as follows:

$$\hat{x} = y - \hat{n} \tag{2}$$

The mean squared error (MSE) is chosen as the loss function to optimize the network parameters, leading to optimal denoising performance. The expression for MSE is given by:

$$MSE = \frac{1}{2M} \sum_{i=1}^{M} (\hat{n}_i - (y_i - x_i))^2 \tag{3}$$

where $(y_i - x_i)_{i=1}^{M}$ is a set of M pure noise sets used for training.

2.2. Network Model

To address the issue of effective signal loss, an RD-SAUNet model is established to attenuate random noise in microseismic data. The network architecture is shown in Figure 1. The RD-SAUNet is a symmetrical end-to-end network, which mainly contains five structures: encoder blocks, skip connections, max pooling, upsampling, and decoder blocks. Four convolutional blocks are used in the encoding and decoding stages to extract the waveform features of noisy data and reconstruct denoised data. Each encoder block contains seven hidden layers: two convolutional layers, two batch normalization (BN) layers, two nonlinear activation layers, and an RSAM module. The decoder similarly contains seven hidden layers: two convolutional layers, two BN layers, two nonlinear activation layers, and a 1×1 convolutional layer. To further enhance noise suppression, the dilation rate progressively increases in the downsampling encoder and correspondingly decreases in the upsampling decoder.

The specific structural design is as follows:

In CNNs, more contextual information is acquired by enlarging the receptive field. Inspired by this, this paper uses dilated convolution to effectively expand the receptive field without increasing computational cost, thereby preserving a greater amount of relevant information within microseismic data [37,38]. If the size of the convolution kernel is defined as $(2r+1) \times (2r+1)$, its convolution operation can be expressed as:

$$S_{i,j} = \sum_{2r+1} \sum_{2r+1} z(i + 2r + 1, j + 2r + 1) \times w(2r + 1, 2r + 1) \tag{4}$$

where z is the input data matrix; w is the convolution kernel; i, j represent the pixel position after the convolution operation, respectively; and r is the coefficient of expansion.

The receptive field size of each dilation convolution is:

$$G_{i+1} = G_i + (k-1)\Pi_{i=1}^{i}\text{stride}(i) \tag{5}$$

where G_{i+1} and G_i are the receptive field sizes of the current layer and the previous layer, respectively; k is the size of the convolution kernel; and stride(i) is the length of the move step.

In microseismic data denoising, extracting suitable features and key information from the dataset is crucial. By learning spatial weights from the input data, the SAM enables the network to emphasize important regions while suppressing irrelevant components [30,39]. The SAM consists of three steps: pooling, concatenation, and convolution. In this paper, the SAM is used to replace the convolutional layer in the residual structure, forming the proposed RSAM, as shown in Figure 2.

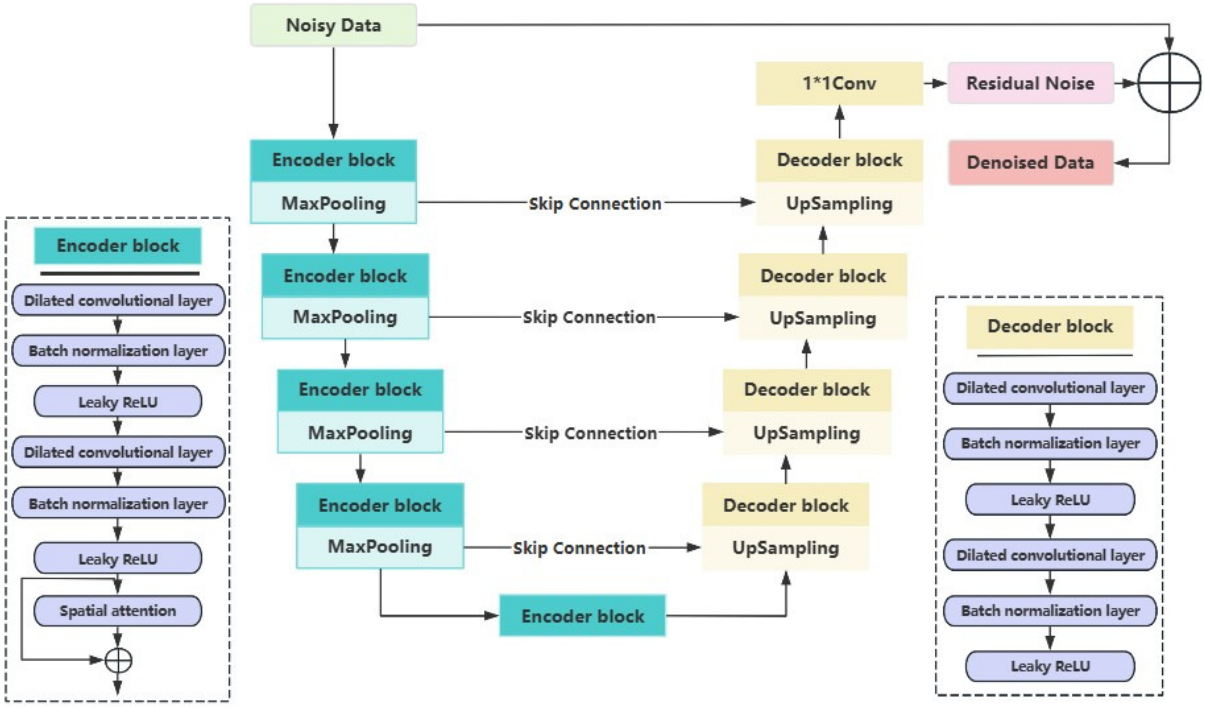

Figure 1. Network Model Structure Diagram.

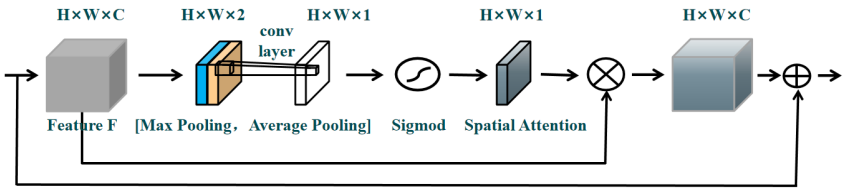

Figure 2. Schematic Diagram of Spatial Attention Model.

The RSAM uses the spatial relationship between input features to generate the spatial attention weight matrix and employs skip connections to enhance the multi-level feature fusion ability of the module, thereby avoiding the loss of key details. Formally, given an input feature map $F \in \mathbb{R}^{H\times W\times C}$, Max Pooling and Average Pooling are applied across the channel dimension, resulting in two output feature maps $F'_{MP} \in \mathbb{R}^{H\times W\times 1}$ and $F'_{AP} \in \mathbb{R}^{H\times W\times 1}$, respectively. These features maps F'_{MP} and F'_{AP} are then concatenated along the channel dimension to yield a combined feature map $F'_2 \in \mathbb{R}^{H\times W\times 2}$ [40]. A convolution operation is subsequently performed on the concatenated feature map to produce a feature map $F'_1 \in \mathbb{R}^{H\times W\times 1}$. The spatial attention weight matrix $M_s(F)$ is then obtained by applying the Sigmoid function, leading to the SAM's output feature map $F^S \in \mathbb{R}^{H\times W\times 1}$ [41]. Finally, the output F_{RSAM} of the RSAM is obtained by element-wise addition of F^S and the original input F. This process can be formulated as follows:

$$\begin{aligned} F_{RSAM} &= F^S + F \\ &= F \bullet M_S(F) + F \\ &= F \bullet \theta(f^{7\times7}([MP(F); AP(F)])) + F \\ &= F \bullet \theta(f^{7\times7}([F'_{MP}; F'_{AP}])) + F \end{aligned} \tag{6}$$

where $f^{7\times7}$ is the convolution operation whose convolution kernel size is 7×7; and θ is the Sigmoid activation function.

After the convolutional layer, a BN layer is introduced to standardize the output from the convolution. This normalization process ensures that the input data for each subsequent layer approximates a consistent normal distribution [32,42]. Additionally, it helps mitigate the problem of internal covariate shift caused by changes in the distribution of the input data [43,44].

3. Experiments

3.1. Performance Metrics

In this article, the SNR and structural similarity index (SSIM) are predominantly employed as quantitative evaluation metrics to assess the denoising performance on microseismic data [45,46]. SNR and SSIM are widely utilized evaluation indices. Among these metrics, SNR directly quantifies the extent of noise suppression, whereas SSIM assesses the degree of distortion and similarity in the waveform characteristics of the denoised signal compared to the clean signal. These metrics are described as follows.

$$\text{SNR} = 10\text{lg}\frac{x^2}{(x-\hat{x})^2} \tag{7}$$

$$\text{SSIM}(x,\hat{x}) = \frac{(2\mu_x\mu_{\hat{x}} + C_1)(2\sigma_{x\hat{x}} + C_2)}{(\mu_x^2 + \mu_{\hat{x}}^2 + C_1)(\sigma_x^2 + \sigma_{\hat{x}}^2 + C_2)} \tag{8}$$

where x and $\hat{x}$ are the original microseismic signal and the denoised microseismic signal, respectively; μ_x and σ_x^2 are the mean and variance of x, respectively; $\mu_{\hat{x}}$ and $\sigma_{\hat{x}}^2$ are the mean and variance of $\hat{x}$, respectively; $\sigma_{x\hat{x}}$ is the covariance of x and $\hat{x}$; and C_1 and C_2 are constants used to maintain stability. The SSIM ranges from 0 to 1, and its value equals 1 when x and $\hat{x}$ are identical. Higher SNR and SSIM values indicate a better denoising effect of the method.

3.2. Experimental Setup

During training, the Adam (Adaptive Moment Estimation) optimizer is employed to minimize the loss function. This optimizer adjusts the learning rate based on the error computed from previous epochs, thereby accelerating convergence. The initial learning rate is set to 0.001, with a total of 50 training epochs. The batch size is set to 20, and the input and output sizes of the model are both set to 60×200. The experiments were conducted on a 64-bit operating system with an Intel Core i5 processor, 16GB of RAM, and a quad-core CPU. The GPU utilized in this configuration is Intel(R) Iris(R) Xe Graphics. The software uses Python 3.11 and PyTorch to build the deep learning framework.

For synthetic data, an 8:1:1 ratio is utilized for training, validation, and testing, respectively, with clean data serving as the labels. To enhance dataset diversity, varying levels of random noise are introduced to the synthetic microseismic data records, creating a training dataset that encompasses both the signal set and the noise set. The Ricker wavelet is employed to generate synthetic signals via forward modeling on a two-layer velocity model. This process yields 60 synthetic seismic records. The predominant frequency is set to 50 Hz, and the sampling interval is 1 ms, as shown in Figure 3. Figure 3a depicts clean microseismic data, while Figure 3b displays noisy microseismic data with an SNR of 1.16 dB. RD-SAUNet was first tested on synthetic microseismic data, and its performance was analyzed and compared with other methods in this study.

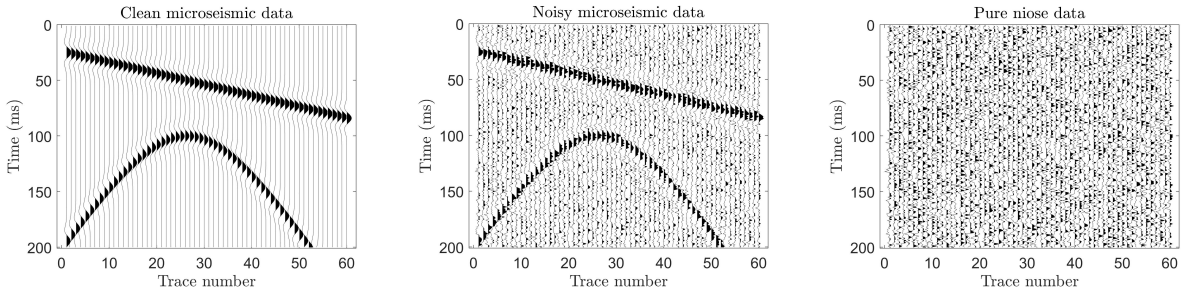

(a) Clean data. (b) Noisy data. (c) Pure noise data.

Figure 3. Sythetic data.

3.3. Ablation Experiments

To verify the impact of the dilated convolution block and the improved attention mechanism in the RD-SAUNet denoising model on overall performance, ablation experiments and analysis were conducted. It mainly includes four models: U-Net; U-Net with hybrid dilated convolutions (DU-Net); U-Net with hybrid dilated convolutions and a standard SAM (DSAU-Net); and U-Net with hybrid dilated convolutions and the proposed RSAM (i.e., RD-SAUNet). The training losses and SNR of the four network models are shown in Figure 4, with the black, red, green, and blue curves corresponding to their respective experimental results. As shown in Figure 4a, the training loss of RD-SAUNet not only has the smallest initial value but also remains consistently lower than those of the other three methods and stabilizes as it decreases. As shown in Figure 4b, as the number of epochs increases, the SNR of the network model containing RSAM is on average 1 dB higher than that of the models with SAM and other variants.

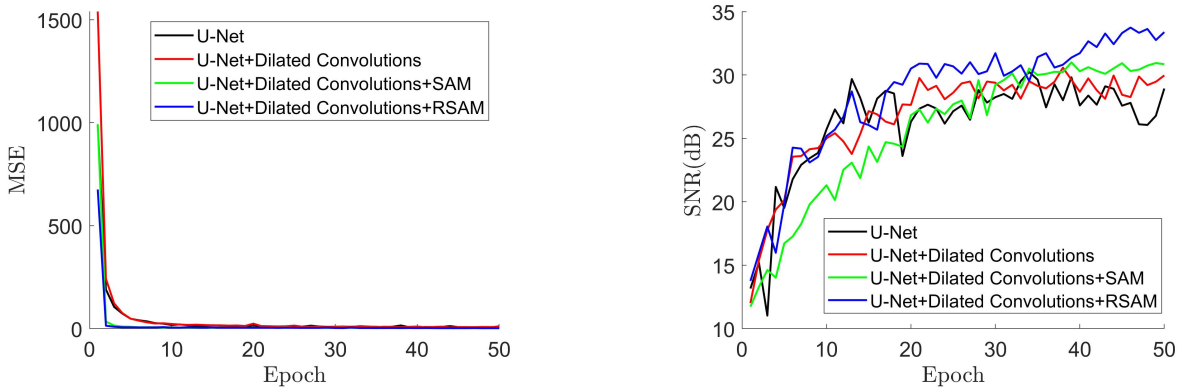

(a) Training loss of different methods. (b) SNR.

Figure 4. Training loss and SNR curves of different methods.

Table 1 summarizes the influence of different module combinations on the noise reduction effect of the test set. From Table 1, it can be seen that the SNR of the ablation model U-Net is the lowest, indicating that the two blocks play an important role in the denoising effect of the RD-SAUNet model. Compared with the RD-SAUNet model, the SNR of the ablation model DU-Net decreased by 1.95 dB, the SNR of the ablation model DSAU-Net decreased by 1.42 dB. This indicate that deleting any of the dilated convolutions and SAM will significantly reduce the denoising effect of the network. Compared with the original SAM, the improved SAM increased the SNR by 1.42 dB, indicating that the improved SAM has a significant denoising effect on the RD-SAUNet denoising model.

Table 1. Results of the ablation experiments on the RD-SAUNet network

	Dilated Convolutions	**SAM**	**RSAM**	**SNR/dB**	**SSIM**
U-Net	×	×	×	17.74	0.9669
DU-Net	√	×	×	18.02	0.9673
DSAU-Net	√	√	×	18.55	0.9782
RD-SAUNet	√	×	√	19.97	0.9899

3.4. Comparative Experiments

This paper applies denoising procedures to the previously mentioned synthetic noisy microseismic records using WPT, DnCNN, U-Net, and the proposed method. First, as illustrated in Figure 5a, the WPT denoising method achieves only partial noise suppression, leaving the effective signal substantially corrupted, which poses significant challenges for subsequent tasks such as microseismic first-arrival picking and source localization. As illustrated in Figure 5b, DnCNN effectively suppresses complex background noise; however, a significant number of effective signal components can still be observed in its residual noise profile shown in Figure 5f. Figure 5c presents the results after applying U-Net, which clearly demonstrates a strong denoising performance, exhibiting almost no residual noise and well-preserved microseismic signals. Nevertheless, examining the corresponding residual noise profile in Figure 5g reveals that discernible portions of effective signals are still present in the filtered noise. Although both DnCNN and U-Net show notable effectiveness in suppressing random noise, the method proposed in this paper exhibits superior performance in both noise attenuation and preservation of signal details, as demonstrated in Figure 5d and Figure 5h. Furthermore, Figure 5i, Figure 5j, Figure 5k, and Figure 5l display the local similarity maps computed between the clean and denoised microseismic data for each method. These maps reveal varying degrees of signal detail loss across the different approaches. Notably, the local similarity map produced by the proposed method achieves a higher energy value of 0.9899 compared to the other methods, indicating that the algorithm effectively suppresses random noise while preserving the fine characteristics of the original microseismic signals.

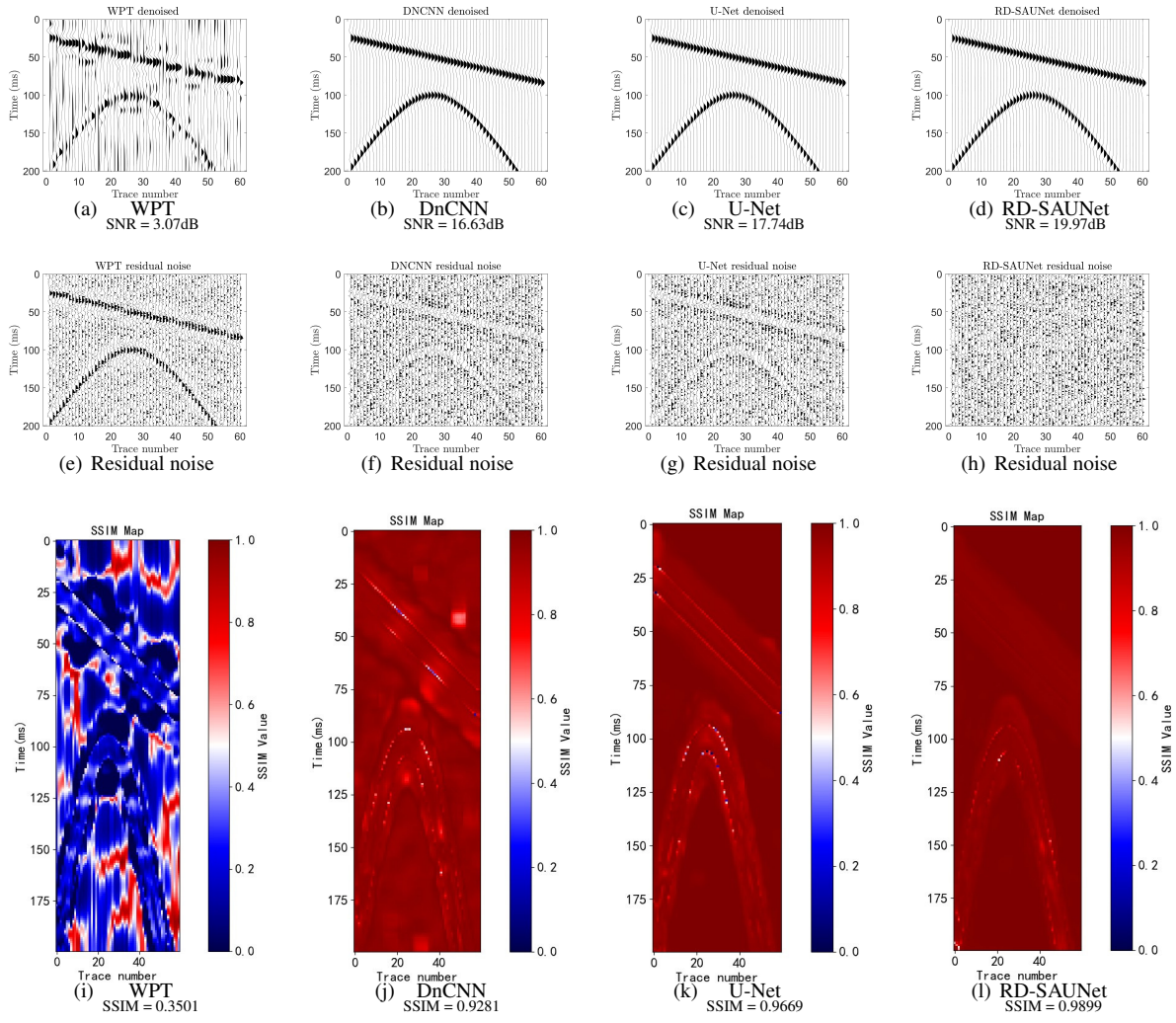

Figure 5. Noise reduction results by different methods.

To evaluate the denoising performance in detail, Figure 6 presents the first recorded signal extracted from the denoised results, enabling a comparative analysis of denoising outcomes across different methods. The microseismic signal obtained using the method proposed in this paper exhibits a higher degree of alignment with the clean reference signal after noise reduction. Moreover, Table 2 provides a quantitative assessment of the noise suppression capabilities of various methods under different noise intensities on the same test set. The results demonstrate that the proposed method achieves superior generalization performance in denoising microseismic data across a range of noise levels.

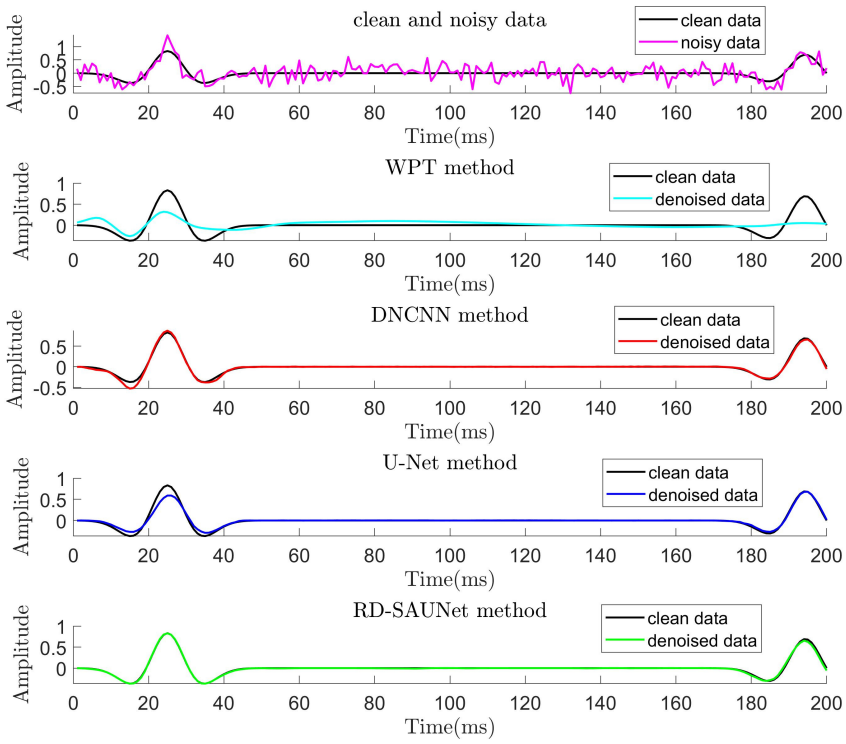

Figure 6. Denoised results of single trace.

Table 2. Comparison of network model noise reduction parameters

Noise Level SNR/dB	Algorithm	SNR/dB	SSIM
−1.77	WPT	1.05	0.1556
	DnCNN	12.58	0.7912
	U-Net	16.80	0.9764
	RD-SAUNet	17.92	0.9664
0.09	WPT	1.76	0.2080
	DnCNN	16.12	0.9095
	U-Net	17.54	0.9697
	RD-SAUNet	19.63	0.9866
2.87	WPT	4.02	0.4031
	DnCNN	18.93	0.9385
	U-Net	20.89	0.9797
	RD-SAUNet	21.10	0.9881

3.5. Synthetic Records with Field Noise

To evaluate the denoising performance of the RD-SAUNet model on different types of noise and microseismic data, we generated clean signals by performing forward modeling using a Ricker wavelet on a two-layer velocity model, as shown in Figure 7a. To simulate realistic field conditions, field noise samples are extracted from microseismic recordings devoid of events and superimposed onto clean signals to evaluate the model's denoising performance under realistic field conditions, as depicted in Figure 7b. This was done to test the denoising effectiveness of the method under complex noise environments. Each microseismic trace in the dataset comprises 200 sampling points with a 1-ms sampling interval. The denoising results are presented in Figure 8.

Figure 8a presents the denoised result obtained by the WPT method. The waveform exhibits low resolution and weak phase energy, indicating that the effective signal remains inadequately recovered. Although DnCNN and U-Net can effectively suppress random noise, the two methods above still exhibit traces of residual noise. For example, as depicted in Figure 8b, after DnCNN noise reduction, the effective signal has a certain degree of signal distortion. As shown in Figure 8c, after denoising by U-Net method, the noise signal is regarded as an effective signal in the first and third trace. In contrast, the denoised results of this article proposed RD-SAUNet method closely resemble the simulated signal record, and the residual profile is devoid of noticeable remnants of effective

signals within the filtered noise.

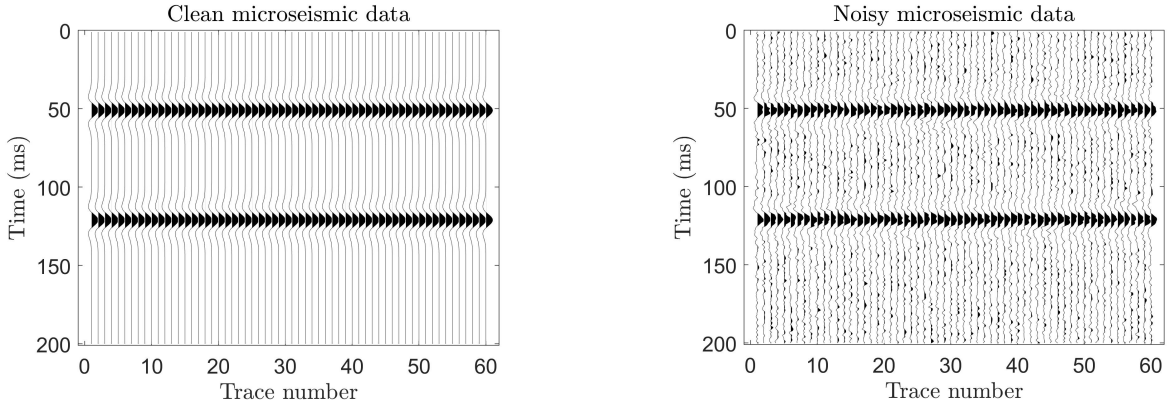

(a) Clean microseismic data. (b) Noisy microseismic data.

Figure 7. Synthetic records with field noise.

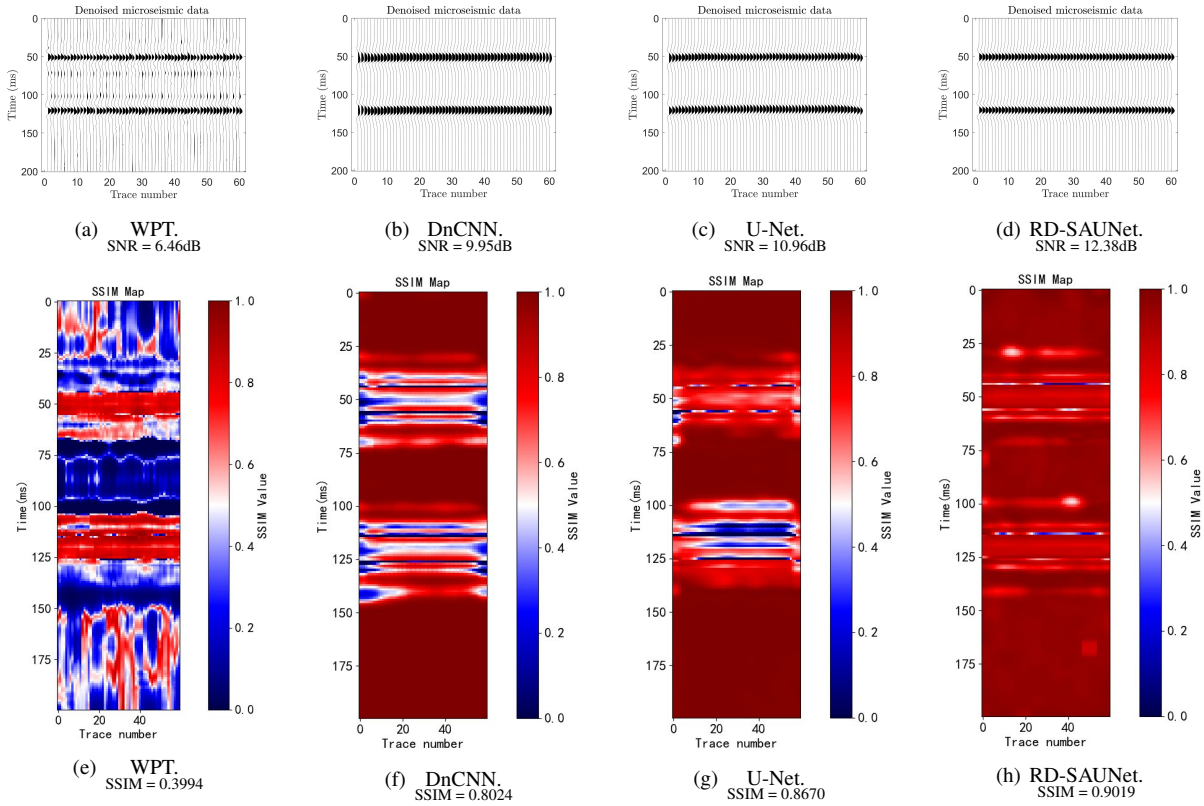

(a) WPT. SNR = 6.46dB (b) DnCNN. SNR = 9.95dB (c) U-Net. SNR = 10.96dB (d) RD-SAUNet. SNR = 12.38dB

(e) WPT. SSIM = 0.3994 (f) DnCNN. SSIM = 0.8024 (g) U-Net. SSIM = 0.8670 (h) RD-SAUNet. SSIM = 0.9019

Figure 8. Field noise reduction results by different methods.

For a more comprehensive assessment of noise attenuation procedure using these methods, the local similar maps are calculated between the clean and denoised data, as depicted in Figure 8e–h. The above three methods, WPT, DnCNN, and U-Net, have a better denoising effect for real noise. However, multiple anomalous points of noise still exist, signifying somewhat impairment to the signal. Notably, the similarity map after WPT denoising reveals localized noise residuals and blurred phase-axis information,as shown in Figure 8e. In contrast, as depicted in Figure 8h, this article proposed method exhibits higher efficacy in suppressing field noise and preserving the effective signal.

4. Actual Microseismic Data

To evaluate the reliability of the proposed method, the three aforementioned denoising algorithms are applied to real-world noisy microseismic data. Figure 9 displays field-collected microseismic records from a region in Northeast China. The inherently complex subsurface environment, influenced by various factors, gives rise to noise signals characterized by broad frequency bands and intricate spectral components. The noise exhibits complicated

waveform features, variable amplitudes, and highly irregular patterns, which collectively obscure the effective microseismic signals. These noise sources primarily include construction-related noise, impulsive noise, equipment-induced vibration noise, and mixed noise. The noise displays significant amplitude fluctuations, with complex frequency components distributed across high-, medium-, and low-frequency bands.

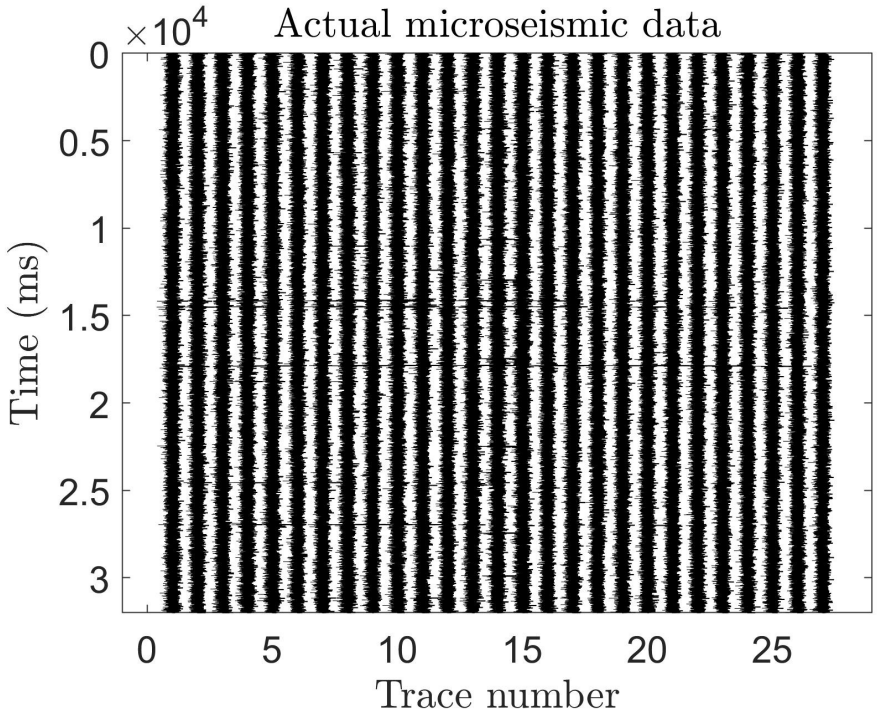

Figure 9. Multievent microseismic data.

When employing deep learning techniques for denoising seismic and microseismic data, a fixed input and output size is commonly adopted, which compromises the integrity of the original data. When the length of the raw data exceeds the model's predefined input dimensions, it must be forcibly truncated—thereby disrupting the temporal continuity of the signal. It is well recognized that the duration of microseismic events to be monitored varies randomly, making a fixed-size approach poorly adaptable to practical engineering requirements. To enhance the applicability of this proposed method in real-world scenarios, this article adopts a cropping and block-based processing strategy during the preprocessing stage. Such a strategy enables effective processing of data with arbitrary lengths while preserving data integrity and avoiding signal distortion caused by truncation. To mitigate signal distortion caused by overlapping regions during splicing, weighted averaging is applied at the seams, thereby preserving the integrity of microseismic data before and after denoising.

Formally, the data is first partitioned into smaller blocks, where the original microseismic signal is segmented and cropped into manageable sub-units of a specified size (the dimensions of which can be flexibly defined). For segments that do not meet the required size, appropriate padding operations are applied. The pre-trained denoising model is then applied to each individual block. Upon completion of the denoising process, the original data size is recovered through a reconstruction procedure that takes into account the initial block dimensions and the stride used during segmentation.

Figure 10 presents the denoising results of different methods. The four methods can achieve a relatively good denoising effect, and the waveform distortion is relatively small. The data denoised by the WPT method exhibits substantial noise residuals, low resolution, and poor overall quality as depicted in Figure 10a. As shown in Figure 10b and Figure 10c, although both the DnCNN and U-Net methods mitigate the noise, the two algorithms have significantly damaged the signal integrity, resulting in disruption of the in-phase axis continuity. Specifically, after denoising by DnCNN method, effective signal loss occurs near the 18,000 sampling points from 23 to 27 channels. The U-Net method loses the effective signal amplitude to a large extent near the 18,000 sampling point, which makes subsequent event recognition difficult. In addition, both methods lose a large number of effective signals near the 25,000 sampling point, resulting in the loss of microseismic events and degrading the accuracy of source localization. In comparison, as shown in Figure 10d, the denoising effect of the method proposed in this paper is clearly better, and the overall waveform is clearer.

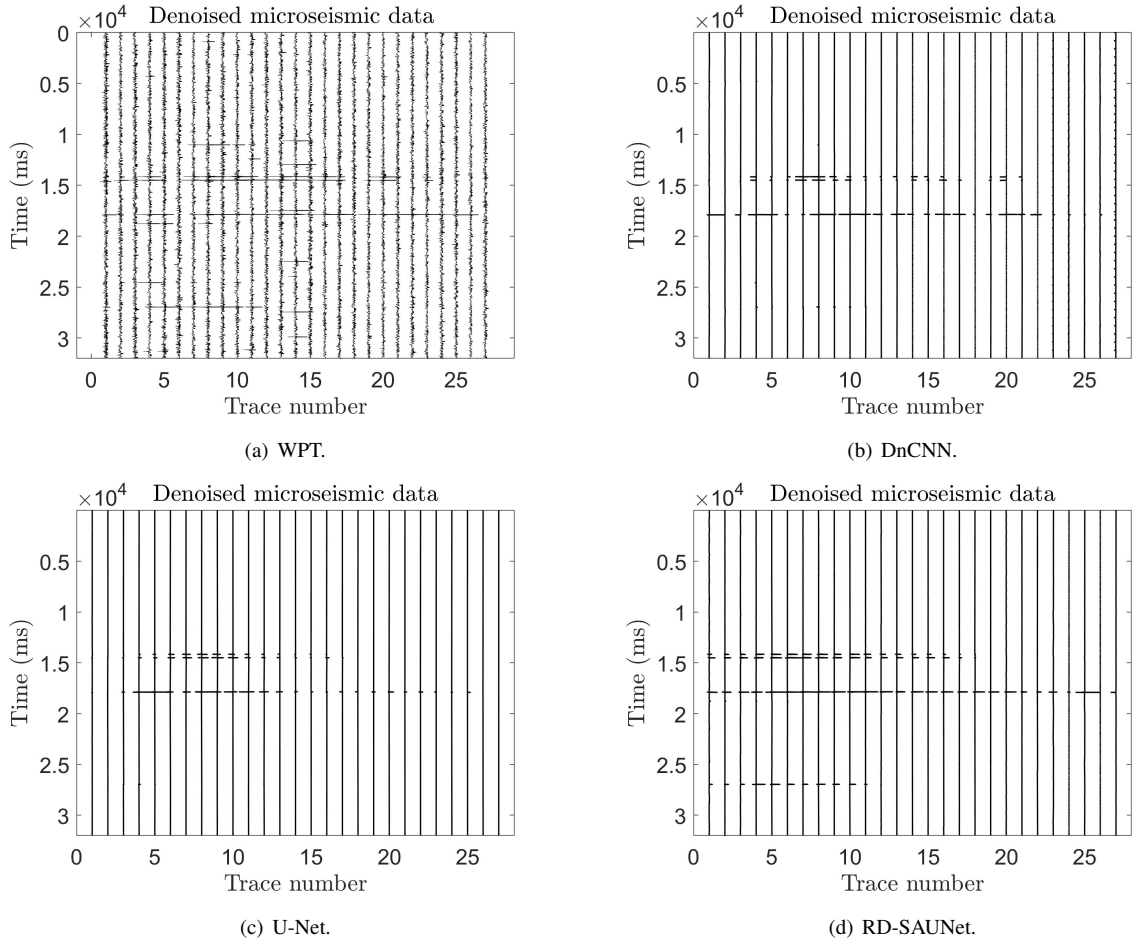

(a) WPT. (b) DnCNN.

(c) U-Net. (d) RD-SAUNet.

Figure 10. Denoising comparison for different methods.

To further examine the denoising performance in detail, the fourth trace was extracted from the denoising results for a comparative analysis across different methods, as shown in Figure 11. Figure 11a displays the single-channel microseismic signal denoised by the WPT method. Although random noise is partially suppressed, considerable interference remains. As shown in Figure 11b,c, both the U-Net and DnCNN methods improve signal quality to some extent. However, after applying these approaches, a significant amount of noise remains and noticeable signal energy loss is observed. In contrast, the method proposed in this paper, illustrated in Figure 11d, effectively suppresses noise while preserving fine signal details and maintaining signal energy stability. Notably, it successfully attenuates noise prior to the arrival of both P-waves and S-waves, which is advantageous for subsequent microseismic data processing.

To systematically evaluate the denoising performance of various models on real microseismic signals, the stability of phase attributes is adopted as a quantitative metric. This metric measures the ability of the noise reduction method to preserve the characteristics of the original signal by comparing multiple attributes of the signal before and after noise reduction. Among them: amplitude stability reflects whether the energy of the signal after noise reduction is overly weakened or amplified; frequency consistency focuses on whether noise reduction causes frequency domain distortion and avoids the loss of effective frequency components; polarization stability is used to test the impact of noise reduction on the polarization characteristics of the wave field and ensure the accuracy of polarization information; waveform consistency measures the similarity between the waveform shape after noise reduction and the original signal. By integrating these attributes, the applicability and fidelity of the noise reduction model on actual microseismic data can be comprehensively evaluated through a radar chart. When the score reaches above 0.5, it indicates a good denoising effect, providing a reliable basis for the quantification of the denoising effect. As shown in Figure 12, the proposed method achieves a score of 0.591, demonstrating that the microseismic signals are effectively enhanced across multiple dimensions, including amplitude, frequency, polarization, and waveform, resulting in a significant improvement in overall signal quality.

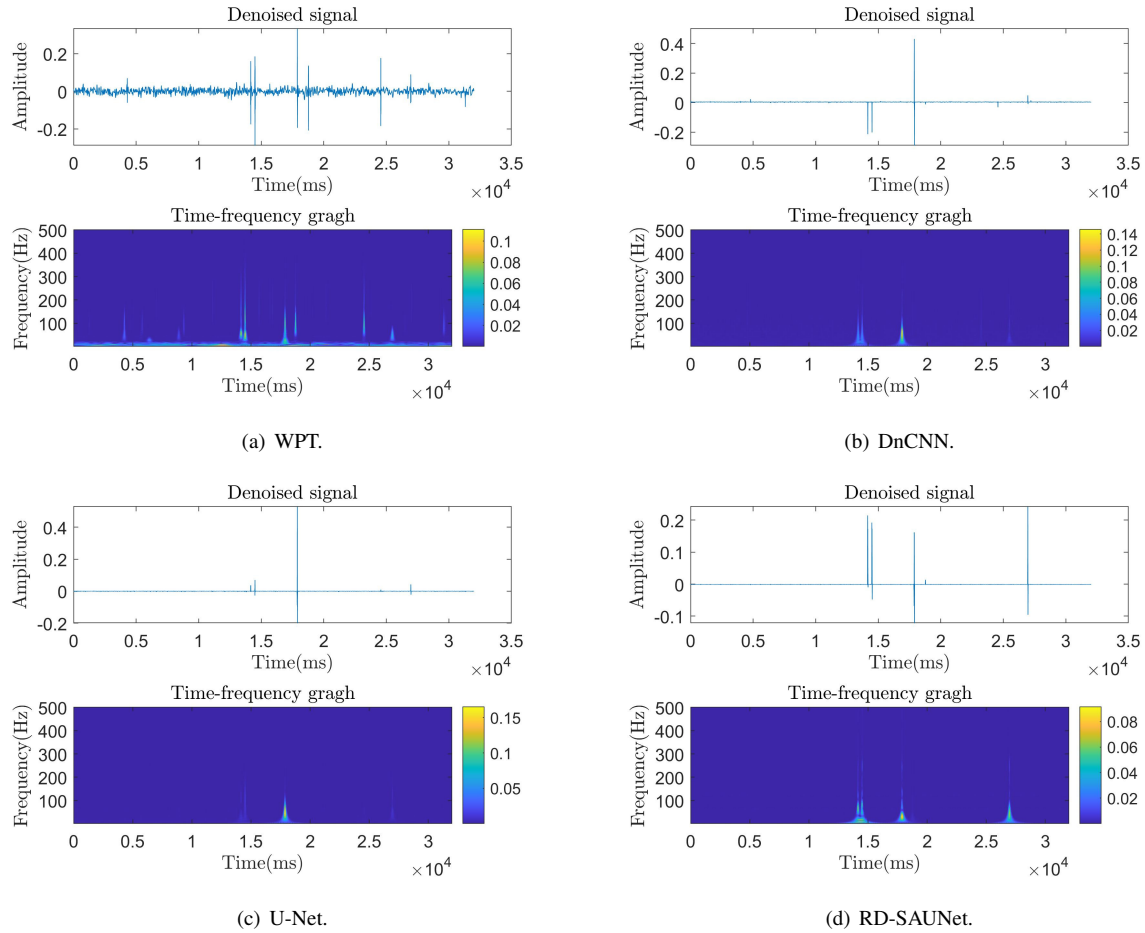

(a) WPT.

(b) DnCNN.

(c) U-Net.

(d) RD-SAUNet.

Figure 11. Results in the time-frequency domain.

Tests were performed on a single microseismic event from the same survey area to evaluate the stability of the proposed algorithm, as illustrated in Figure 13. Figure 14a illustrates the denoising result obtained by the WPT method. Most of random noise is effectively suppressed, and the underlying microseismic signal becomes progressively clearer. However, considerable low-frequency interference persists between channels, particularly prior to the P-wave arrival. Such residuals can lead to misidentification during subsequent first-arrival picking, where the P-wave may be erroneously classified as noise-ultimately resulting in event loss. The denoising results from DnCNN and U-Net are shown in Figure 14b,c, respectively. While both methods improve the clarity of coherent events in the microseismic data, they also lead to the loss of detailed signal information, particularly around channel 15, where significant amplitude attenuation is observable. In contrast, as shown in Figure 14d, the RD-SAUNet method achieves more effective noise suppression, enhances phase continuity, minimizes signal loss, and produces a clearer and more discernible event.

A single trace was randomly selected for comparison to more clearly illustrate the changes in microseismic signals before and after denoising, as shown in Figure 15. Figure 15a presents the microseismic signal after WPT denoising. The result shows limited noise suppression, with noisy interference remaining in the denoised signal. The denoising results of the DnCNN and U-Net methods are shown in Figure 15b,c, respectively. While both approaches remove a significant amount of random noise, they struggle to suppress low-frequency noise effectively. The waveform and time–frequency diagrams reveal that substantial low-frequency noise remains, accompanied by a loss of effective signal energy. In contrast, as shown in Figure 15d, the proposed method not only suppresses high- and low-frequency noise more effectively but also preserves signal integrity and maintains more stable energy levels in the denoised output.

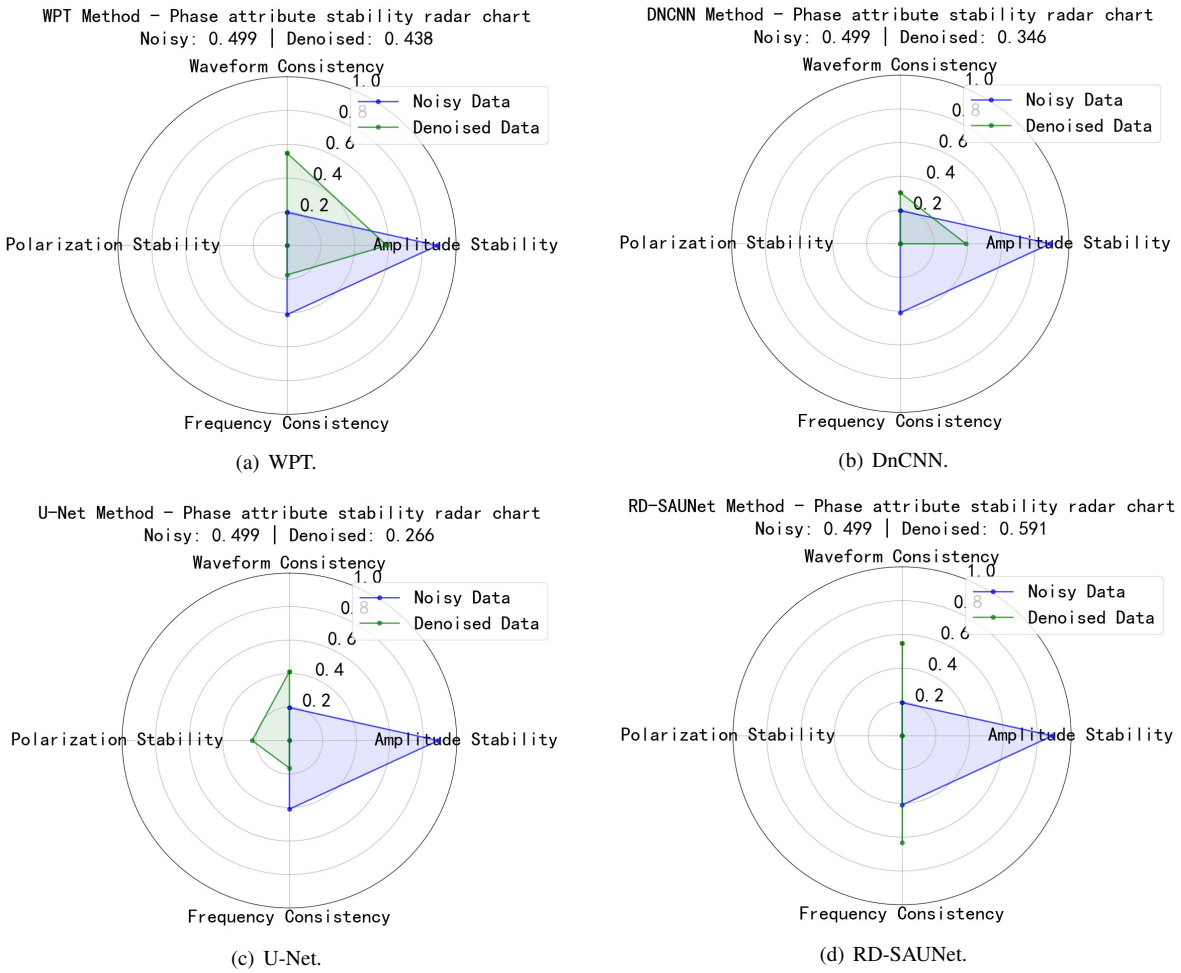

(a) WPT. (b) DnCNN.

(c) U-Net. (d) RD-SAUNet.

Figure 12. Comparison of phase attribute stability after noise reduction by different methods.

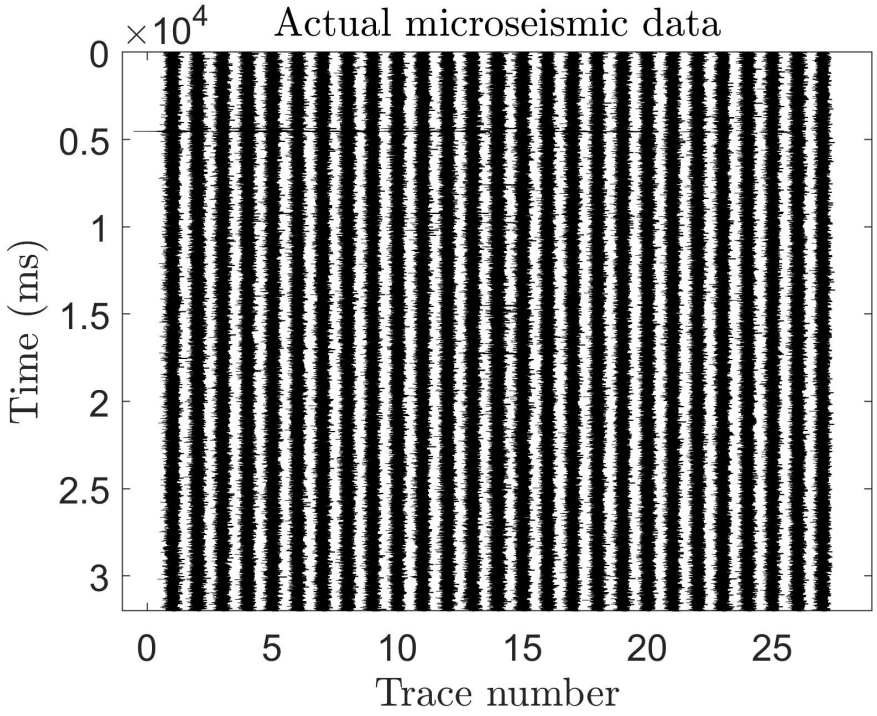

Figure 13. Single-event microseismic data.

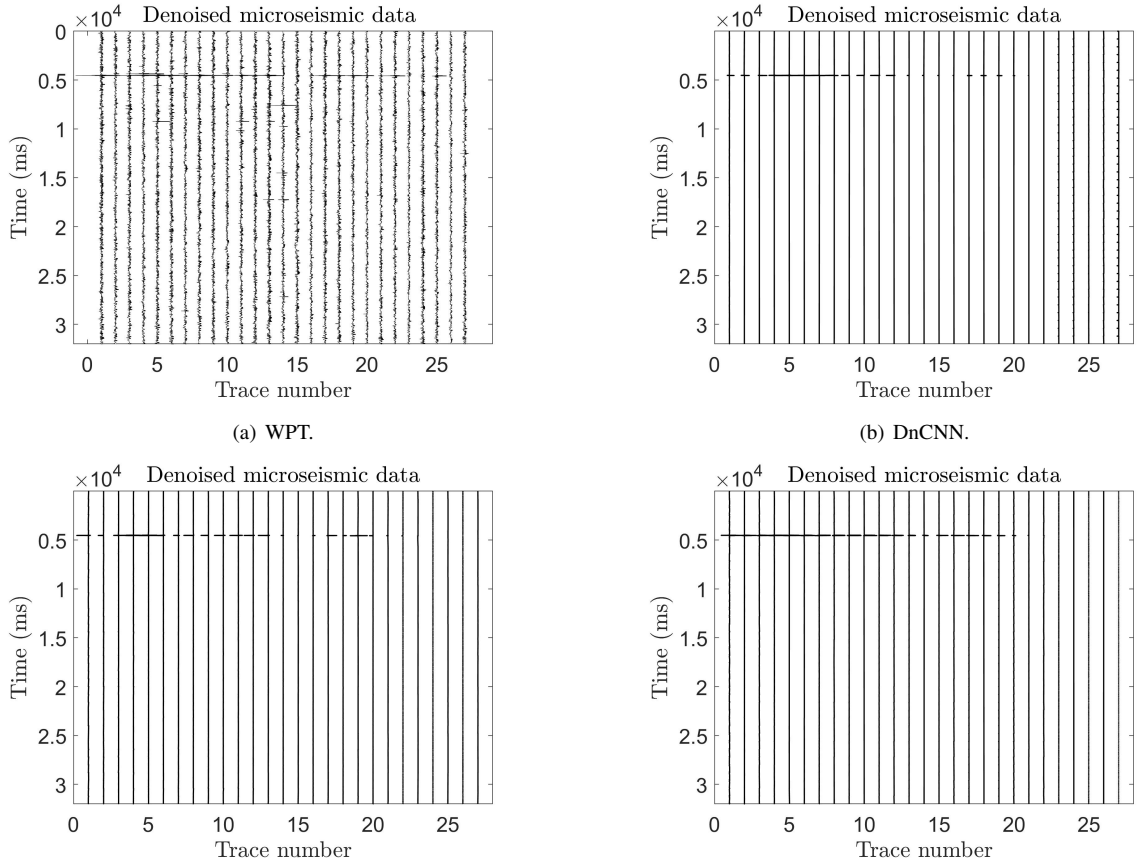

(a) WPT. (b) DnCNN.

(c) U-Net. (d) RD-SAUNet.

Figure 14. Denoising comparison for different methods.

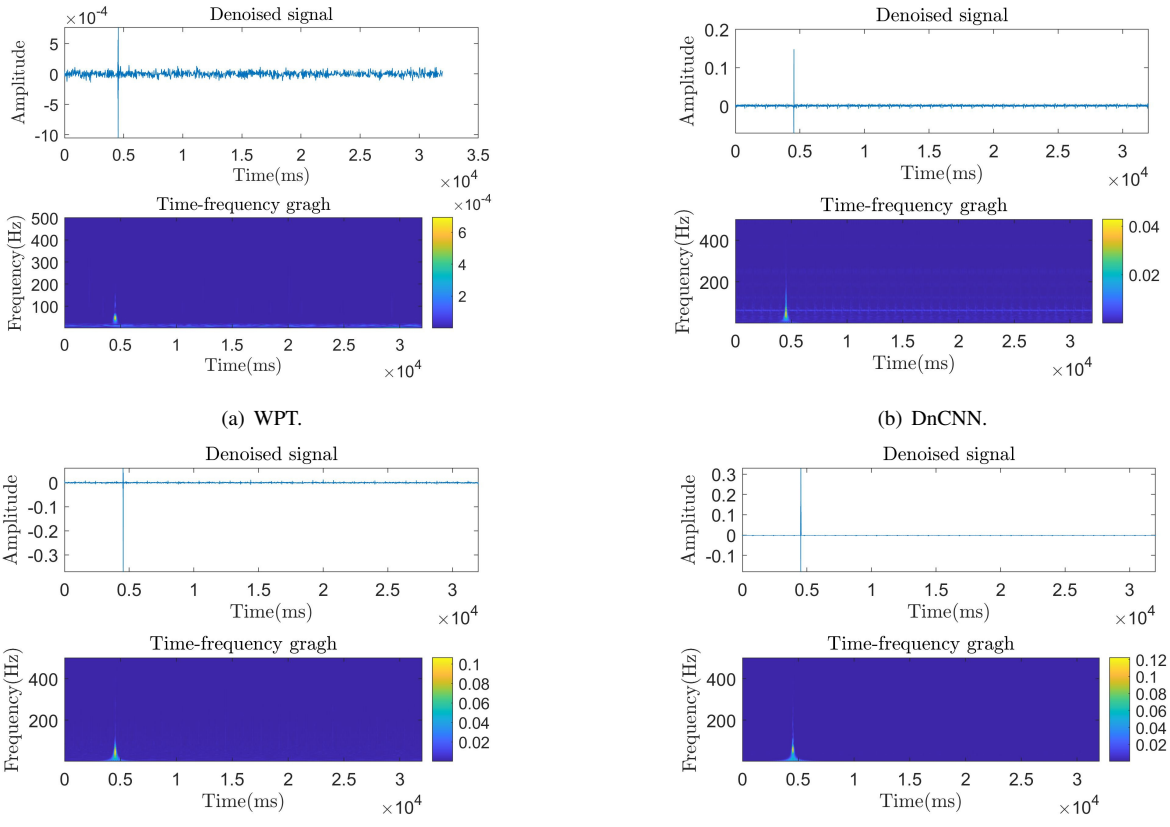

(a) WPT. (b) DnCNN.

(c) U-Net. (d) RD-SAUNet.

Figure 15. Results in the time-frequency domain.

5. Conclusions

Based on the standard U-Net architecture, a denoising model for microseismic data has been developed by incorporating hybrid dilation convolution, residual structure, and a SAM. The model effectively preserves the fine details of microseismic signals without adding more convolutional layers or altering kernel sizes, thanks to the use of hybrid dilation convolutions. The integration of a RSAM further improves denoising accuracy by dynamically adjusting the importance of different spatial regions in the input data. By weighting features according to their significance, the model enhances both training stability and efficiency. Comparative experiments with existing models such as WPT, DnCNN and the standard U-Net show that the proposed RD-SAUNet-based denoising algorithm substantially increases the SNR. This improvement is of great significance for subsequent tasks, such as first-arrival picking, source localization, and inversion imaging of microseismic waves. In practical testing, the model supports block processing and reconstruction, enabling real-time denoising of microseismic data with arbitrary time-window lengths. This approach prevents truncation artifacts caused by fixed-size inputs and maintains signal integrity, making it well-suited for real-world engineering applications with variable data sizes. Experiments demonstrate that the proposed model adapts better to realistic noise conditions, reducing residual and signal distortion. These results confirm the strong generalization performance of the model across different types of noise.

Although the denoising model proposed in this study performs well on synthetic microseismic data, residual noise persists between traces during field microseismic data testing. Future work will focus on enhancing the complexity and diversity of the training dataset by incorporating varying levels of non-uniform noise during training. This approach is expected to improve the model's generalization ability and noise suppression performance in practical applications. Another limitation is the high parameter count of the proposed denoising model, which adversely affects computational efficiency. To mitigate this issue, future work will investigate lightweight model design strategies —such as network pruning and knowledge distillation —with the aim of reducing model complexity while preserving denoising performance, thereby enhancing the model's practicality in field microseismic data applications.

Author Contributions: H.C. (Huashuai Cui): conceptualization, methodology, software, data curation, writing—original draft preparation, visualization, investigation, and validation; F.H.: conceptualization, methodology, software, data curation, writing—original draft preparation, supervision, and writing—review and editing; H.C. (Huanjun Chen): visualization and investigation; Y.S.: supervision and writing—review and editing. All authors have read and agreed to the published version of the manuscript.

Funding: This work was supported in part by in part by the National Natural Science Foundation of China under Grants U21A2019.

Institutional Review Board Statement: Not applicable. This study does not involve humans or animals.

Informed Consent Statement: Not applicable. This study does not involve human subjects.

Data Availability Statement: The synthetic training dataset and field measurement data generated in this study are proprietary to our research group and are not publicly available due to ongoing research considerations. However, they can be made available from the corresponding author upon reasonable request.

Conflicts of Interest: The authors declare no conflict of interest.

Use of AI and AI-Assisted Technologies: No AI tools were utilized for this paper.

References

1. Birnie, C.; Ravasi, M.; Liu, S.; et al. The potential of self-supervised networks for random noise suppression in seismic data. *Artif. Intell. Geosci.* **2021**, *2*, 47–59.
2. Gao, H.Y.; Zhang, M.; Hou, N.; et al. Dynamic-transmission-based recursive filtering algorithm for microseismic event detection under sensor saturations. *Measurement* **2021**, *186*, 110197.
3. Guan, C.; Zheng, L.; Wang, C. A novel CEEMD-based multichannel denoising autoencoder for noise attenuation of surface microseismic data. *Int. J. Netw. Dyn. Intell.* **2025**, *4*, 100026.
4. Fomel, S.; Liu, Y. Seislet transform and seislet frame. *Geophysics* **2010**, *75*, V25–V38.
5. Liu, S.; Wang, L.; Zhang, Y.; et al. Recursive filtering of networked systems with communication protocol scheduling: A survey, *Int. J. Syst. Sci.* **2025**, *56*, 2499–2516.
6. Zhang, Y.; Liu, G.; Song, X. Unscented recursive three-step filter based unbiased minimum-variance estimation for a class of nonlinear systems. *Int. J. Syst. Sci.* **2025**, *56*, 227–236.
7. Zhi, Y.-L.; Wu, Y.-Y.; Zhang, Y.; et al. A new result on reachable set estimation for Markovian jump neural networks with time-varying delays. *Int. J. Syst. Sci.* **2025**, *56*, 4131–4143.

8. Meng, C.; Gao, J.; Tian, Y.; et al. Attenuation of seismic random noise with unknown distribution: A gaussianization framework. *IEEE Trans. Geosci. Remote. Sens.* **2023**, *61*, 5915915.
9. Mousavi, S.M.; Langston, C.A. Hybrid seismic denoising using higher-order statistics and improved wavelet block thresholding. *Bull. Seismol. Soc. Am.* **2016**, *106*, 1380–1393.
10. Labate, D.; Lim, W.-Q.; Kutyniok, G.; et al. Sparse multidimensional representation using shearlets. In *Wavelets XI*; SPIE: Bellingham, DC, USA. 2005; pp. 254–262.
11. Han, J.; van der Baan, M. Microseismic and seismic denoising via ensemble empirical mode decomposition and adaptive thresholding. *Geophysics* **2015**, *80*, KS69–KS80.
12. Zhang, X.; Cao, L.; Chen, Y.; et al. Microseismic signal denoising by combining variational mode decomposition with permutation entropy. *Appl. Geophys.* **2022**, *19*, 65–80.
13. Mousavi, S.M.; Langston, C.A.; Horton, S.P. Automatic microseismic denoising and onset detection using the synchrosqueezed continuous wavelet transform. *Geophysics* **2016**, *81*, V341–V355.
14. Zhu, W.; Zhang, C.; Qiu, T.; et al. The seismic signal technology with variable velocity FK filtering-the auto-adapted polarization filtering. *Prog. Geophys.* **2009**, *24*, 1776–1786.
15. Tselentis, G.-A.; Martakis, N.; Paraskevopoulos, P.; et al. Strategy for automated analysis of passive microseismic data based on S-transform, Otsus thresholding, and higher order statistics. *Geophysics* **2012**, *77*, KS43–KS54.
16. Song, B.; Zhao, S.; Dang, L.; et al. A survey on learning from data with label noise via deep neural networks, *Syst. Sci. Control. Eng.* **2025**, *13*, 2488120.
17. Zhan, Y.; Yang, R.; You, J.; et al. A systematic literature review on incomplete multimodal learning: techniques and challenges. *Syst. Sci. Control. Eng.* **2025**, *13*, 2467083.
18. Lin, J.; Zheng, J.; Li, D.; et al. Research on microseismic denoising method based on CBDNet. *Artif. Intell. Geosci.* **2023**, *4*, 28–38.
19. Zhang, Y.; Li, X.; Wang, B.; et al. Robust seismic data denoising based on deep learning. *Oil Geophys. Prospect.* **2022**, *57*, 12–25.
20. Wang, Y.; Wen, C.; Wu, X. Fault detection and isolation of floating wind turbine pitch system based on Kalman filter and multi-attention 1DCNN. *Syst. Sci. Control. Eng.* **2024**, *12*, 2362169.
21. Liu, L.; Song, W.; Zeng, C.; et al. Microseismic event detection and classification based on convolutional neural network. *J. Appl. Geophys.* **2021**, *192*, 104380.
22. Mandelli, S.; Lipari, V.; Bestagini, P.; et al. Interpolation and denoising of seismic data using convolutional neural networks. *arXiv* **2019**, arXiv:1901.07927
23. Han, W.; Zhou, Y.; Chi, Y. Deep learning convolutional neural networks for random noise attenuation in seismic data. *Geophys. Prospect. Pet.* **2018**, *57*, 862–869.
24. Yang, L.; Chen, W.; Liu, W.; et al. Random noise attenuation based on residual convolutional neural network in seismic datasets. *IEEE Access* **2020**, *8*, 30271–30286.
25. Zheng, J.; Jiang, T.; Wu, Z.; et al. Application of residual learning to microseismic random noise attenuation. *Acta Geophys.* **2021**, *69*, 1151–1161.
26. Wang, Y.; Lu, W.; Liu, J.; et al. Random seismic noise attenuation based on data augmentation and CNN. *Chin. J. Geophys.* **2019**, *62*, 421–433.
27. Luo, R.; Li, Y. Random seismic noise attenuation based on RUNet convolutional neural network. *Geophys. Prospect. Pet.* **2020**, *59*, 51–59.
28. Zhang, H.; Ma, C.; Pazzi, V.; et al. Microseismic signal denoising and separation based on fully convolutional encoder–decoder network. *Appl. Sci.* **2020**, *10*, 6621.
29. Chen, H.; Wu, R.; Tao, C.; et al. Multi-scale class attention network for diabetes retinopathy grading. *Int. J. Netw. Dyn. Intell.* **2024**, *3*, 100012.
30. Chen, L.; Wu, P.; Tan, W.; et al. A novel UAV-based road damage detection algorithm with lightweight convolution and attention mechanism. *Int. J. Netw. Dyn. Intell.* **2025**, *4*, 100025.
31. Chun, W.; Xu, Y.; Li, Z.; et al. Attention-guided CNN for image denoising. *Neural Netw.* **2020**, *124*, 117–129.
32. Yang, C.; Zhou, Y.; He, H.; et al. Global context and attention-based deep convolutional neural network for seismic data denoising. *Geophys. Prospect. Pet.* **2021**, *60*, 751–762.
33. Ehab, W.; Huang, L.; Li, Y. UNet and variants for medical image segmentation. *Int. J. Netw. Dyn. Intell.* **2024**, *3*, 100009.
34. Chen, H.; Gao, J.; Gao, Z.; et al. A sequential iterative deep learning seismic blind high-resolution inversion. *IEEE J. Sel. Top. Appl. Earth Obs. Remote. Sens.* **2021**, *14*, 7817–7829.
35. Bai, T.; Zhao, H.; Wang, Z. A U-Net based deep learning approach for seismic random noise suppression. In Proceedings of the IGARSS 2022—2022 IEEE International Geoscience and Remote Sensing Symposium, Kuala Lumpur, Malaysia, 17–22 July 2022; pp. 6165–6168.
36. Saad, O.M.; Oboue, Y.A.S.I.; Bai, M.; et al. Self-attention deep image prior network for unsupervised 3-D seismic data enhancement. *IEEE Trans. Geosci. Remote. Sens.* **2021**, *60*, 5907014.
37. Yu, F.; Koltun, V. Multi-scale context aggregation by dilated convolutions. *arXiv* **2015**, arXiv:1511.07122.

38. Zhang, Y.; Li, X.; Wang, B.; et al. Random noise suppression of seismic data based on joint deep learning. *Oil Geophys. Prospect.* **2021**, *56*, 9–25.
39. Zagoruyko, S.; Komodakis, N. Paying more attention to attention: Improving the performance of convolutional neural networks via attention transfer. *arXiv* **2016**, arXiv:1612.03928.
40. Woo, S.; Park, J.; Lee, J.-Y.; et al. Cbam: Convolutional block attention module. In Proceedings of the European Conference on Computer Vision (ECCV), Munich, Germany, 8–14 September 2018; pp. 3–19.
41. Guo, C.; Szemenyei, M.; Yi, Y.; et al. Sa-UNet: Spatial attention U-Net for retinal vessel segmentation. In Proceedings of the 2020 25th International Conference on Pattern Recognition (ICPR), Milan, Italy, 10–15 January 2021; pp. 1236–1242.
42. Shirrmeister, R.T.; Springenberg, J.T.; Fiederer, L.D.J. Deep learning with convolutional neural networks for EEG decoding and visualization. *Hum. Brain Mapp.* **2017**, *38*, 5391.
43. Chen, T.; Yi, Y. Random noise suppression of seismic data based on deep convolution neural network. *Acta Seismol. Sin.* **2021**, *43*, 474–482.
44. López, V.; Fernández, A.; Herrera, F. On the importance of the validation technique for classification with imbalanced datasets: Addressing covariate shift when data is skewed. *Inf. Sci.* **2014**, *257*, 1–13.
45. Chen, J.; Chen, G.; Li, J.; et al. Efficient seismic data denoising via deep learning with improved mca-scunet. *IEEE Trans. Geosci. Remote. Sens.* **2024**, *62*, 5903614.
46. Wang, Z.; Bovik, A.C.; Sheikh, H.R.; et al. Image quality assessment: from error visibility to structural similarity. *IEEE Trans. Image Process.* **2004**, *13*, 600–612.